Chemical Engineering Science 65 (2010) 6443–6451

Contents lists available at ScienceDirect

Chemical Engineering Science

journal homepage: www.elsevier.com/locate/ces

Modeling nano-particle deposition in diesel engine filters

Alfredo Soldati *,[1], Marina Campolo, Fabio Sbrizzai

Centro Interdipartimentale di Fluidodinamica e Idraulica and Dipartimento di Energetica e Macchine, Università di Udine, 33100 Udine, Italy

ARTICLE INFO

Article history:
Received 4 November 2009
Received in revised form
9 August 2010
Accepted 23 September 2010
Available online 29 September 2010

Keywords:
Diesel particulate filter
Soot deposition
Filtration
Mathematical modelling
Particle
Fluid mechanics

ABSTRACT

In this work, we develop a simple, fully analytical one-dimensional model based on lubrication theory to predict nano-particle deposition along the unit channel of a clean diesel particulate filter. Soot deposition along the channel depends on filter design parameters, which can be optimally selected to minimize the uneven distribution of soot. At the initial stage of the filtration process, the porous wall resistance is controlling; at later stages, the local resistance of the deposited soot is controlling. Typically, a hundredfold increase in filter resistance may be observed over time, and the maximum variability in the soot deposition is observed at the initial stages of the process. Therefore, in this work, we focus on the deposition of soot in a clean filter, focusing on the one dimensional variability along the main flow direction. In a clean filter, the porous wall resistance can be considered uniform along the filter length and the flow field and nano-particle transport equations can be solved analytically. Model predictions compare surprisingly well with those obtained from more complex three-dimensional simulations, thereby demonstrating that the essential physics is captured correctly. Based on the very simple framework identified in this paper, more complex models can be developed and used to predict the filter behavior over time (i.e. build-up of the soot cake and back-pressure rise up to the regeneration step) provided that (i) the variation in time of filter permeability due to local soot loading is implemented and (ii) equations are solved numerically.

1. Introduction

Wall-flow filters used to separate nano and micro particles from an exhaust gas of diesel engines are made of a bundle of channels separated by porous ceramic walls, as sketched in Fig. 1. Soot laden gas enters the filter from the engine-side (dirty channels), flows through the porous wall of the channel leaving soot particles deposited at the filter surface and inside the porous material, and exits from clean channels. Deposited soot accumulates progressively over time, enhancing filtration efficiency at the beginning of the filtering process (cake filtration effect). At later stages, the growing thickness of the soot cake leads to an undesired increase of pressure drop through the filter, which may have detrimental effect on engine performances. At this stage, the filter must be regenerated by burning the soot particles constituting the cake, so that the filtration cycle can start again.

Optimally designed diesel particulate filters (DPF) should guarantee high collection efficiency of soot particles (nano and micro size) and low pressure drop for the longer time possible before filter regeneration is required. The uneven, local accumulation of soot inside the filter, which builds up during the early stages of filtration, can be minimized by choosing "ad hoc" at the design stage those filter characteristics which control soot deposition pattern in the clean filter. The more homogeneous the deposition at the initial stage, the more uniform will be the soot loading inside the channel over time, leading to steady performances of the filter.

Recent literature flourishes with papers, mostly based on experimental methods, in which different filters have been tested and compared to identify the best performing. Pressure drop, filtration efficiency and regeneration frequency have been measured experimentally (see Saracco et al., 1999; Saracco et al., 2000; Ambrogio et al., 2001; Fino et al., 2002; Fino et al., 2003; Konstandopoulos and Papaioannou, 2008 among others), together with other filter characteristics like the thermal stability of the catalyst and the complex oxidation dynamics of the soot layer under different operating conditions (see Pidria et al., 2007; Bensaid et al., 2009b; Chen et al., 2009a, b). A significant effort has also been devoted to the development of predictive models able to simulate the pressure drop, the filtration characteristics and the properties of the filter and the soot layer (see Shende et al., 2005), with the final aim of controlling the filter behavior over time (see Dabhoiwala et al., 2008). Experimental data and numerical models are extremely useful to assess the performances of different DPFs and yet have not be used to devise strategies for filter design optimization, as required by the challenging limitations imposed for emission control.

* Corresponding author. Tel.: +39 432 558020; fax: +39 432 558027.
E-mail address: soldati@uniud.it (A. Soldati).
[1] Also at CISM—Centro Internazionale di Scienze Meccaniche, 33100 Udine, Italy.

0009-2509/$ - see front matter © 2010 Elsevier Ltd. All rights reserved.
doi:10.1016/j.ces.2010.09.030

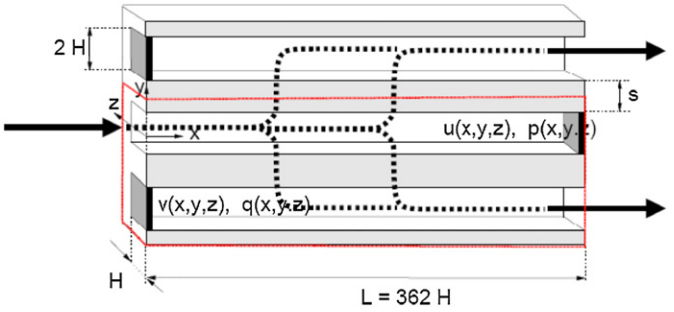

Fig. 1. Sketch of minimal filter unit of DPF. One half of dirty and clean channel is shown together with the reference coordinate system.

Ultimately, filter performances depend upon (i) the characteristic of the filter material (porous wall and deposited soot) and on (ii) the distribution of the flow across the filtering surface. Filter performances are expected to change smoothly over time if the filter works under homogeneous fouling conditions. Significant breakthroughs for filter design optimization can be expected from a deep knowledge of the mechanisms controlling particle transport and deposition *inside* the filter channel. There is experimental and numerical evidence that particle deposition inside a square channel is inhomogeneous both along the spanwise and streamwise directions (see Sharma and Phares (2006) and Phares and Sharma (2006)). A more complex behavior is expected when flow filtration through the wall is possible. Due to the complexity of experimental investigations (Ambrogio et al., 2002; Yang et al., 2009) and the effort underlying numerical computations (Schejbal et al., 2009; Liu et al., 2009) it is hard to find works in the literature investigating particle dynamics and deposition *along* single channels of a porous filter. Yet, it is clear that, due to the small aspect ratio (spanwise/streamwise dimension) of the single channels, particle deposition *has* dynamics in the longitudinal direction.

In our previous papers, we simulated numerically the three-dimensional fluid and particle behavior of the flow approaching a DPF (Sbrizzai et al., 2004; Sbrizzai et al., 2009) and entering a clean filter channel (Sbrizzai et al., 2005). We were able to simulate the uneven distribution of particles at the inlet section of the filter, the preferential accumulation of particles in the corners of the square channel, and to assess, virtually free of semplificative assumptions, the influence of the Brownian force on the deposition rates of nano-particles inside the filter channels. Specifically, in Sbrizzai et al. (2005) we have shown that (i) deposition of nano-particle is non-homogeneous in the spanwise direction and along the filter length, (ii) deposition is controlled by the local through-flow and (iii) Brownian diffusion has negligible effect on nano-particle deposition pattern.

Recently, Bensaid et al. (2009a, 2010) used an Eulerian–Eulerian approach to model the flow and particle behavior in a wall-flow filter operating at different working conditions. Their numerical results confirm the non-homogeneous spatial distribution of particles along the filter length. Yet, they do not predict the very low values of soot concentration we found at the inlet of the channel, most likely due to the contraction of the flow downstream the inlet section, which has been confirmed by other authors (see Liu et al., 2009). Bensaid et al. (2009a, b) also show experimental profiles of soot layer thickness along the filter, which confirm the variation of soot thickness along the channel length. Unfortunately, no experimental measurements are available near the inlet and for the early stages of the filtering process to compare with our numerical results.

Computational models based on three-dimensional Navier–Stokes equation (either Eulerian–Lagrangian or Eulerian–Eulerian) are powerful tools to study the details of the filter flow. Yet, their computational cost prevents the extensive use of numerical simulation for filter design optimization.

In this paper, we identify a very simple framework based on lubrication theory, which can be used to set up model equations to describe the soot filtration process. We derive a fully *a-priori* theoretical, one-dimensional model based on the fluid balance equation and on the particle transport equation. The model is developed with reference to the minimal filter unit shown in Fig. 1 and is assessed against our previous fully resolved three-dimensional simulation (Sbrizzai et al., 2005). The derived set of equations is solved analytically to predict particle deposition rates in an initially clean filter, or when the filter permeability is homogeneous in space. The model can be easily implemented in a design procedure and may be used to predict particle deposition rates *as a function of filter design parameters* in a rather broad range of conditions (i.e. gas flow rate, channel size, porous wall permeability). The early stage deposition controls the build-up of the soot cake, and therefore also the smooth evolution of filter properties over time.

In industrial realization of wall-flow filters, thousands of minimal filter units are arranged in a periodic array to build the entire filter. The dimension of the channel, the number of channels and the choice of the filtering material are design parameters, which may have a significant effect on final filter performances. In this paper, we show that the model developed can be used to perform sensitivity analyses to identify a priori a subset of "best performing" clean filter configurations, which can be investigated in details using more complex tools. Based on the same model equations, a more complex numerical procedure can be implemented to simulate the transient behavior of the filter (i.e. build-up of the soot cake and back-pressure rise up to the regeneration step), provided that the variation in time of filter permeability due to local soot loading is considered and a numerical solution to model equations is found.

2. Theoretical model

The model is derived for the unit element of the filter, half of which is identified by a gray line in Fig. 1. We assume that the flow coming from the engine is distributed uniformly to the DPF section such that the pressure drop along and the flow rate across each unit element is the same. As demonstrated by Bensaid et al. (2009b), this condition can be achieved by the proper design of the filter casing, preventing any abrupt expansion of the flow in front of the filter.

The geometry of the dirty and clean channels which form the unit element of the filter is characterized by a small aspect ratio, $\varepsilon = 2H/L \ll 1$. In similar geometries, the lubrication theory can be used to simplify the balance equations which describe the flow. The reference coordinate system is indicated in Fig. 1 for the dirty channel: x is the streamwise direction (along the channel), y and z are the spanwise and vertical directions. The channel walls are located at $y, z = \pm H$.

The model is based on the following assumptions:

- the geometry is essentially two-dimensional, with y and z both representing wall-normal coordinates; we will refer to the y coordinate as the wall-normal coordinate;
- the flow inside each channel is laminar and incompressible;
- even if the wall is porous, the flow can be described by self-similar Poiseuille velocity profiles; the flow rate decreases along the dirty channel and increases along the clean channel due to the through-wall filtration;
- the flow through the porous wall is proportional to the local pressure drop, as prescribed by the Darcy equation;
- soot nano-particles are carried as a passive non-inertial species by the fluid, i.e. the particle flow is proportional to the fluid flow.

Indicating with $u(x, y)$, ($v(x, y)$), the axial component of velocity and with $p(x, y)$, ($q(x, y)$) the static pressures inside the dirty (clean) channel, according to the lubrication theory Navier–Stokes equations can be simplified as follows:

$$0 = -\frac{\partial p}{\partial x} + \mu \frac{\partial^2 u}{\partial y^2} \tag{1}$$

$$0 = -\frac{\partial p}{\partial y} \tag{2}$$

Eq. (2) indicates that the static pressure is a function of the x coordinate only. In a square channel, the axial component of velocity is a complex function of the wall-normal coordinate y. Yet, to evaluate the variation of flow and particle depositions along the filter channel, we need a relationship between the section averaged value of axial velocity and the pressure drop in the streamwise direction. For simplicity, we will assimilate the velocity profile in the square channel to the velocity profile between two parallel walls. The rigorous derivation for the square channel is discussed in Appendix A. Under this assumption, Eq. (1) can be integrated twice to get the self-similar, Poiseuille velocity profile, which satisfies the no slip boundary condition at the wall:

$$u(x, y) = \frac{1}{2\mu}\left(-\frac{dp}{dx}\right)(y^2 - H^2) \tag{3}$$

where dp/dx is a function of x only.

The section averaged velocity along the channel is given by

$$U(x) = \frac{1}{2H}\int_{-H}^{+H} u(x, y)dy = \frac{H^2}{3\mu}\left(-\frac{dp}{dx}\right) \tag{4}$$

The same velocity profile can be computed also for the clean channel

$$V(x) = \frac{H^2}{3\mu}\left(-\frac{dq}{dx}\right) \tag{5}$$

where $q(x)$ is the static pressure in the clean channel.

The variation of the section averaged velocity along the dirty and clean channels depends on the through-flow across the porous wall. The fluid mass balance for a portion of the dirty/clean channel gives

$$(2H)^2 \frac{dU(x)}{dx} = -4(2H)w(x) \tag{6}$$

$$(2H)^2 \frac{dV(x)}{dx} = +4(2H)w(x) \tag{7}$$

where $w(x)$ is the through-wall velocity, given by Darcy law

$$w(x) = K(p(x) - q(x)) \tag{8}$$

and K is the filter permeability (m/Pa s), which is a function of porous material specific permeability, k_s, wall thickness, s, and fluid viscosity, μ. The filter permeability $K = k_s/\mu s$ can be considered independent of the position along the channel, x, when the filter is clean and when the soot deposition is uniform along the filter length, until the thickness of the soot layer depositing remains negligible with respect to the channel size. Under these conditions, Eqs. (4), (5), (6), (7) and (8) can be rewritten to obtain the following equations:

$$\frac{H^3}{6\mu}\left(\frac{d^2p}{dx^2} + \frac{d^2q}{dx^2}\right) = 0 \tag{9}$$

$$\frac{H^3}{6\mu}\left(\frac{d^2p}{dx^2} - \frac{d^2q}{dx^2}\right) = 2K(p(x) - q(x)) \tag{10}$$

which can be integrated (see Appendix B for details) to obtain the pressure variation along the dirty and clean channel

$$p(x) = \frac{1}{2}(c_1 exp(\lambda x) + c_2 exp(-\lambda x) + c_3 x + c_4) \tag{11}$$

$$q(x) = -\frac{1}{2}(c_1 \exp(\lambda x) + c_2 \exp(-\lambda x) - c_3 x - c_4) \tag{12}$$

where $\lambda = (12K\mu/H^3)^{0.5}$ [1/m]. The value of integration constants c_i, $i = 1, 4$ is found by solving the linear system of equations obtained from the following boundary conditions:

$$p(0) = p_I \quad \text{known pressure @ inlet} \tag{13}$$

$$q(L) = p_E \quad \text{known pressure @ outlet} \tag{14}$$

$$U(L) = -\frac{H^2}{3\mu}\left(\frac{dp}{dx}\right)_L = 0 \quad \text{known axial velocity @ plug} \tag{15}$$

$$V(0) = -\frac{H^2}{3\mu}\left(\frac{dq}{dx}\right)_0 = 0 \quad \text{known axial velocity @ plug} \tag{16}$$

The calculated values of c_i, $i = 1, 4$ are shown in Appendix C. Once the pressure profiles along the two channels are known, the flow inside the unit element of the filter is fully determined: the section averaged velocity profile along the dirty and clean channel is given by Eqs. (4) and (5) and the through-wall flow is given by Eq. (8).

Eq. (4) can also be used to find a useful relationship between the two macroscopic parameters usually monitored in filter tests, i.e. the flow rate, Q, and the pressure drop $\Delta p = p_I - p_E$. The section averaged velocity at the inlet of the dirty channel is given by

$$U(0) = \frac{U_\infty}{R} = \frac{Q}{A_{flow}} \Big/ \frac{A_{flow}}{A_{unit}} \tag{17}$$

where U_∞ is the gas velocity before entering the filter channel and R is the geometrical factor used to describe the contraction of the flow area at the filter inlet.

From Eq. (4), the section averaged velocity at the channel inlet is also given by

$$U(0) = \frac{H^2}{6\mu}(c_1\lambda - c_2\lambda + c_3) \tag{18}$$

These two equations can be re-arranged to give

$$\Delta p = p_I - p_E = RES \cdot U(0) \tag{19}$$

where RES is the filter resistance which is a function of filter geometry (H, s and L), filter material (k_s) and fluid viscosity (see Appendix E for details).

To predict the deposition of soot particles at the filter wall at the initial stages of soot deposition, we write the mass balance for the soot entering the filter

$$\frac{d\dot{m}}{dx} = -4(2H)w(x)C(x) = -\frac{2}{H}\frac{w(x)}{U(x)}\dot{m}(x) \tag{20}$$

where $\dot{m}(x)$ is the soot mass flow rate [kg/s] and $C(x) = \dot{m}(x)/U(x)(2H)^2$, [kg/m^3], is the concentration of soot in the flow. This equation can be integrated to give

$$\dot{m}(x) = \dot{m}(0)\frac{c_1\lambda\exp(\lambda x) - c_2\lambda\exp(-\lambda x) + c_3}{2\lambda(c_1 - c_2)} \tag{21}$$

According to the mass balance, the mass of soot depositing per unit length of the channel is given by

$$\dot{m}_{dep,\ ul}(x) = -\frac{d\dot{m}}{dx} = -\dot{m}(0)\frac{c_1\lambda^2\exp(\lambda x) + c_2\lambda^2\exp(-\lambda x)}{2\lambda(c_1 - c_2)} \tag{22}$$

Eq. (22) predicts that, in a clean filter, the mass of soot depositing per unit length of the channel is a function of the position along the channel length. Experimental data available from the literature and relative to full loaded filters confirm

that the deposition of soot is not uniform inside the filter channel (see Bensaid et al. (2009b, 2010) and Chen et al. (2009b)). In fact, soot deposition patterns change over time depending on the local and instantaneous resistance to through-flow, due to the layer of soot already deposited on the porous wall. It is suggested that the process of local accumulation of soot in specific regions of the filter may be important to explain an uneven variation of filter performances over time. As observed by Chen et al. (2009a and 2009b), the non-uniform spatial distribution of particles may lead, during filter regeneration, to different combustion modes in different parts of the filter, which may eventually lead to differential thermal stresses. We believe that (i) the more homogeneous the deposition at the initial stage of the filtering process, the more uniform will be the soot deposition inside the channel over time, and that (ii) optimal steady performance of the filter can be obtained by a proper design of the filter.

To assess "a priori" how critical can be the control of filter behavior over time, a synthetic measure of dis-homogeneity of soot deposition, i.e. the deviation of the actual deposition profile with respect to the ideal uniform deposition, can be very useful. Based on the local spatial distribution of the soot depositing, we can define the coefficient of variation of the distribution, CV, as

$$CV = \frac{ST.DEV.(\dot{m}_{dep,\ ul}(x))}{E(\dot{m}_{dep,\ ul}(x))} \tag{23}$$

i.e. as the ratio between the standard deviation of the deposition profiles from the average deposition and the average deposition. The larger CV, the larger the dis-homogeneity of soot deposition along the channel wall. According to our model, based on Eq. (22), CV can be calculated as

$$CV = \left[\frac{\lambda L}{8(c_1-c_2)^2}(c_1^2 B(B-2)-c_2^2 A(A-2)+4\lambda c_1 c_2 L)-1\right]^{0.5} \tag{24}$$

where $A=1+\exp(-\lambda L)$ and $B=1+\exp(\lambda L)$.

Given the mass of gas to be filtered and the filter characteristics (geometry and specific permeability), the theoretical model can be used to predict the filter behavior in terms of pressure drop across the filter and variability of the soot deposition profile along the filter. Furthermore, these calculations can be easily made for different design parameters/operating conditions. In this way, the model can be used to perform sensitivity analysis on the effect of filter characteristics/operating conditions on filter performances in the early stages of the filtering process.

The same model equations and boundary conditions can also be used to simulate the transient behavior of the filter during loading conditions, provided that the local changes in filter permeability as a function of the mass of soot deposited are modelled and model equations are integrated numerically.

3. Model validation

There are few experimental data from the literature describing soot deposition pattern during the early stages of the filtration process to validate precisely soot deposition patterns predicted by our analytical model. Experimental measurements of soot cake thickness are typically taken at specific stages of the filtration process performing destructive tests (see, for instance, Bensaid et al., 2010). This is the reason why the initial stages of the deposition process and measuring points close to the inlet section are usually overlooked. Therefore, the ability of the model to predict soot deposition at filter walls has been assessed against two main data sets: (i) part of the data reported in the paper by Bensaid et al. (2010), referring to the early stage of filtration, and (ii) the results of our previous accurate numerical simulation (Sbrizzai et al., 2005), in which we modelled the behavior of a diesel particulate filter installed on a common rail diesel engine car (Fiat 1.9 JTD). Table 1 summarizes geometrical characteristics of the filter and engine working conditions.

The specific permeability of the filter is a quantity, which is hard to measure since it depends on the type and on the grain size of the ceramic material constituting the filter. Table 1 reports values of the permeability of ceramic materials typically used for DPF (see Adler, 2005). In our previous work, the permeability of the filter (unknown) was determined by a trial and error procedure based on the experimental data available on pressure drop evaluated at different engine operating conditions. Specifically, the parameters describing the permeability in Darcy law in the numerical model implementation were gradually modified to fit the experimental data (see Sbrizzai et al., 2005 for details). In this work, the permeability of the filter will be fixed in a similar way, fitting the results of the analytical model with the available experimental data.

The pressure drop measured between the inlet and outlet sections of the filter housing during experimental tests performed at 2000 rpm engine regime (164 kg/h flow rate) was found to be about $\Delta p_{filter}=8$ mbar (see Fig. 4 in Sbrizzai et al., 2005). As reported by Masoudi (2005), filter pressure drop is the sum of four major components: inlet/exit effect, frictional losses and flow through the filtration wall. From our numerical simulation, we found that the contribution of pressure drop between the inlet of dirty channels and the outlet of clean channels was about one third of the overall measured pressure drop Δp_{filter} (i.e. $\Delta p=260$ Pa).

Based on the data in Table 1 and the relationship shown in Appendix E, we can calculate a contraction factor equal to $R=0.31$, a filtering velocity equal to $U_\infty=3$ m/s and the section averaged inlet channel velocity equal to $U(0)=9.7$ m/s.

According to Eq. (19), the value of filter resistance RES matching $U(0)$ under the given pressure drop, Δp, is univocally fixed as shown in Fig. 2, from which the "estimated" specific permeability of the filter, k_s, can be obtained. For the present data, we obtain $k_s=1.47972\times10^{-12}$, which is in the range proposed in the literature (Adler, 2005).

The flow field inside the filter channels is fully determined once k_s is fixed. Fig. 3 shows the variation of pressure, section averaged velocity and through-wall flow calculated by the analytical model. Fig. 3(a) shows the pressure profiles calculated for the dirty (solid line) and clean (dashed line) channels according to Eqs. (11) and (12). The local difference in pressure between the dirty and clean channels is responsible for the through-wall velocity shown in Fig. 3(b) and for the variation of

Table 1
Geometrical characteristics and operative conditions used for filter testing.

Filter data		
Filter diameter	D_f	14.2 cm
Filter length	L	25.34 cm
Channel half-width	H	1.4 mm
Wall thickness	s	0.38 mm
Number of open channels	N_{ch}	2483
Filter specific porosity	k_s	$10^{-12}\div10^{-9}$ m^2[a]
Mass flow rate	$\dot{m}$	164 kg/h
Gas density	ρ	0.965 kg/m^3
Gas temperature	T	600 K
Gas viscosity	μ	2×10^{-5} Pa s
Outlet pressure	p_E	10^5 Pa
Pressure drop (in–out channel)	Δp	260 Pa

[a] From Adler, 2005

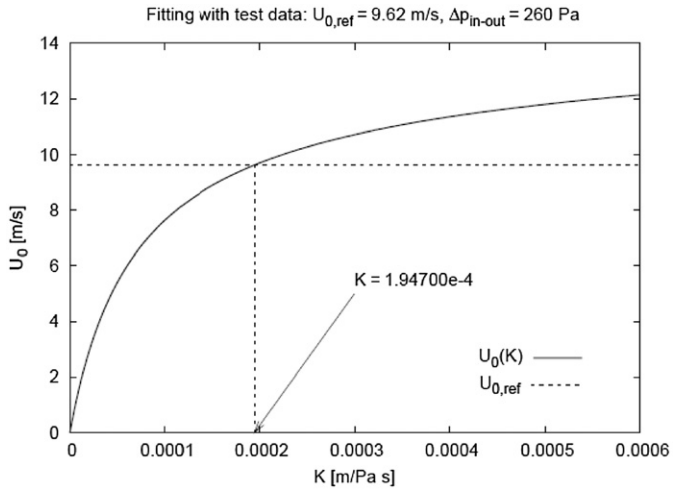

Fig. 2. Mean velocity at channel inlet versus filter permeability K (model fitting equation).

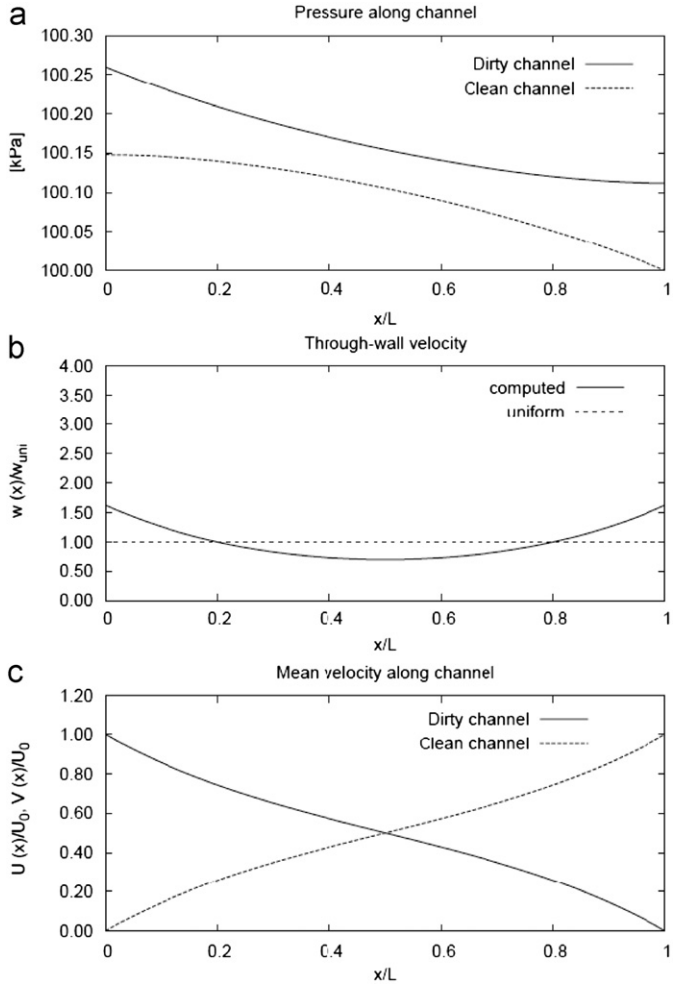

Fig. 3. Variation of pressure and flow along the filter length: (a) pressure profiles along the dirty (solid) and clean (dashed) channel; (b) through-flow along the channel and (c) mean velocity variation along the dirty (solid) and clean (dashed) channel.

the section averaged velocities $U(x)$ and $V(x)$, which decrease along the dirty channel (solid line) and increase along the clean channel (dashed line) as shown in Fig. 3(c).

Fig. 4 shows the effect of the flow field on the soot mass transport. The soot loading decreases along the dirty channel (Fig. 4(a)) proportionally to the gas flow rate. The deposition of soot along the channel wall is not uniform, with symmetric peaks at the inlet and plugged sides of the channel, as expected from the through-wall velocity profile.

Fig. 5 shows the comparison between the through-wall velocity and the soot deposition profile computed by the analytical model (solid) and by the numerical model (dashed) by Sbrizzai et al. (2005). The through-wall velocity profile (Fig. 5(a)) computed by the numerical model (dashed curve) is asymmetric, with a zero flow region right downstream the channel inlet. Larger velocity values are found near the end of the dirty channel. The through-wall velocity calculated by the analytical model is symmetric, with a minimum midway along the channel length. The agreement between the two profiles is rather good. Fig. 5(b) and (c) shows the mass of soot deposited per unit length of the channel computed by the 1 D and the 3 D models. The deposition predicted by the analytical model is proportional to the through-wall velocity. The model cannot predict the reduced deposition of nano-particle at the inlet of the channel, shown in Fig. 5(c), which is due to the local contraction of the flow. This deficiency does not depend on the 1 D assumption and is found also in Eulerian–Eulerian three-dimensional models (see Bensaid et al., 2009a). Some distance downstream the channel inlet, the analytical model can give a precise quantification of the local soot deposition along the channel. The analytical model predicts that the soot layer will be less (75%) than expected in the center of the channel and larger (165%) than expected at the channel ends. These figures are in qualitative agreement with data shown by Bensaid et al. (2009b and 2010). Specifically, data shown in figure 9 by Bensaid et al. (2009b) representing soot deposition evaluated after 7.8 h for a filter housing designed to have a uniform distribution of the flow at the filter inlet (most similar to our case) indicate a relative thickness variation (made dimensionless using the mean thickness value) in the range $\pm 20\%$ at the different measuring points along the channel. These figures are consistent with values predicted by

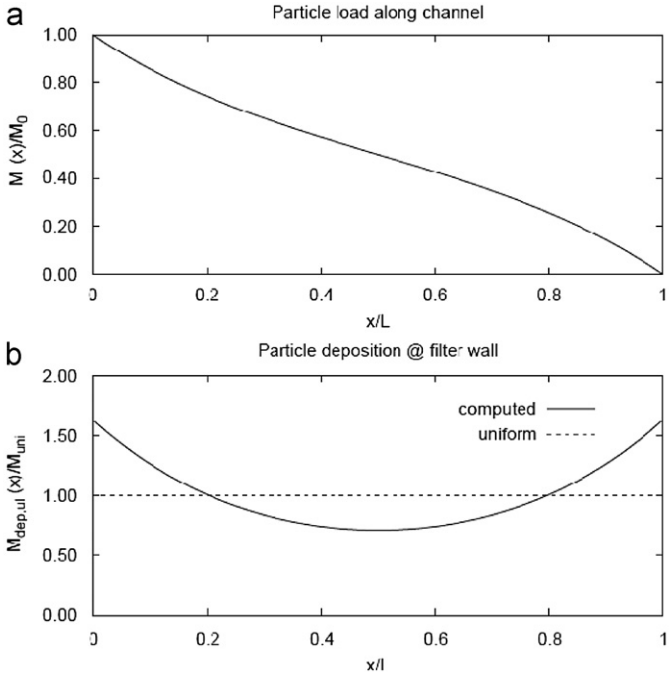

Fig. 4. Variation of (a) particle load along the filter length and (b) particle deposition.

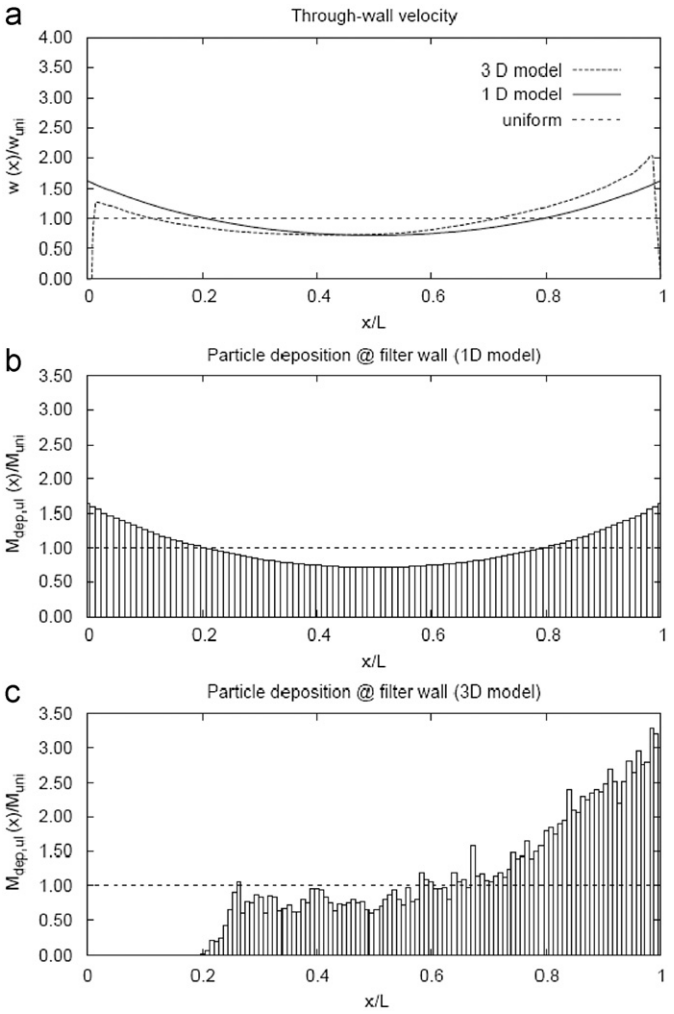

Fig. 5. Model validation: (a) through-wall velocity across porous wall computed by an analytical model (solid) and by three-dimensional numerical simulation (dashed) (Sbrizzai et al., 2005); (b) particle deposition along channel computed by 1 D, analytical model and (c) particle deposition along channel computed by 3 D, numerical simulation (Sbrizzai et al., 2005).

our analytical model in the central portion of the channel. Unfortunately, no measures are available near to the inlet and the outlet of the channel, where the largest deviations from the uniform deposition of soot are expected from the model (about 60%). Data shown in Fig. 2 by Bensaid et al. (2010) corresponding to soot deposition profiles calculated at different stages during the filtering cycle, confirm that in the early stages of soot deposition ($t=0.05$) the spatial variability of the soot layer thickness can be significantly larger than the average, especially at the inlet and outlet ends of the channel.

The dis-homogeneity in soot accumulation calculated by the model can be synthetically described by a coefficient of variation equal to 0.267, i.e. the variation in soot deposition averaged over the filter length is $\pm 27\%$ with respect to the uniform deposition. As discussed previously, this can be a valuable piece of information to improve the control of filter performances.

4. Sensitivity analysis

The analytical model can be efficiently used to assess the variation of clean filter performances (pressure drop, dis-homogeneous spatial distribution of soot), when specific filter characteristics are changed. Since the early stage deposition controls the build-up of the soot cake, filter characteristics indirectly also control the evolution of filter properties over time.

We present in the following two example applications, in which the model is used (i) to identify the "optimal" specific permeability for a filter having a given geometrical configuration, and (ii) to find the "optimal" geometrical configuration of a filter having a given specific permeability.

Fig. 6 shows the variation of filter pressure drop, Δp, and deposited soot coefficient of variation, CV, as a function of the specific permeability of the filter material, k_s. The point represents the pressure drop and CV of the filter examined by Sbrizzai et al. (2005). The functional dependence of pressure drop on k_s indicates that any increase in the specific permeability of the ceramic material will produce a decrease of pressure drop. Yet, the functional dependence of CV on k_s indicates that any increase in the specific permeability of the ceramic material will produce an increase in the dis-homogeneity of deposition. An optimal choice of k_s can thus be made focusing on the most critical issue: minimizing the pressure drop at the expense of a more dis-homogeneous deposition of soot or vice versa promoting the more homogeneous deposition of soot at the expense of a larger pressure drop.

Fig. 7 shows the variation of filter pressure drop and deposited soot coefficient of variation as a function of the number of open filtering channels into which a given filter section can be divided. In this case, we assume that the overall volume available to install

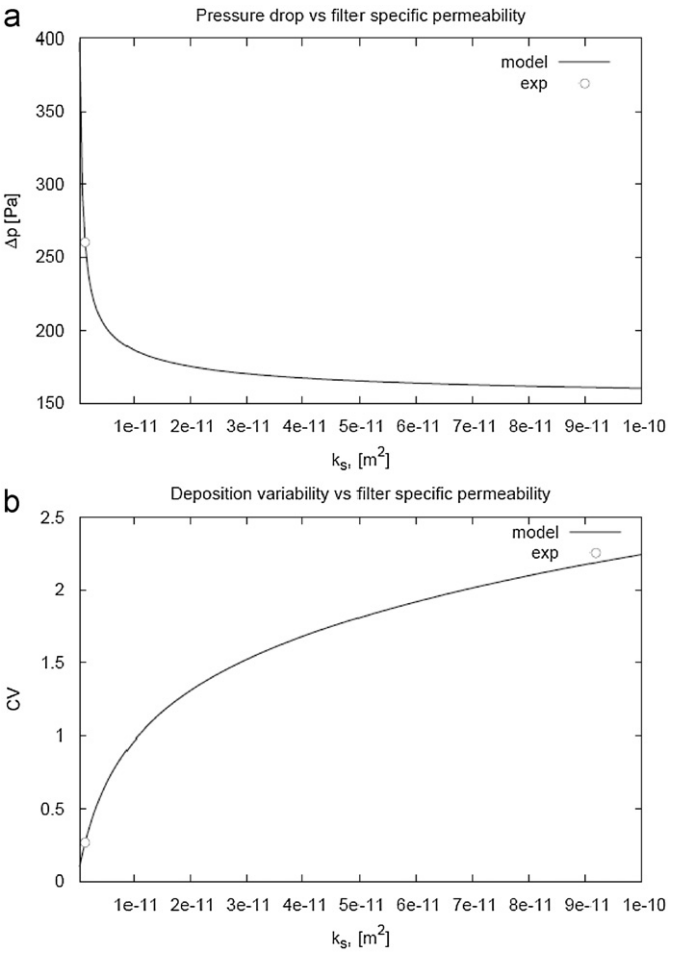

Fig. 6. Effect of filter specific permeability on filter performances: (a) pressure drop and (b) variability of deposition along filter.

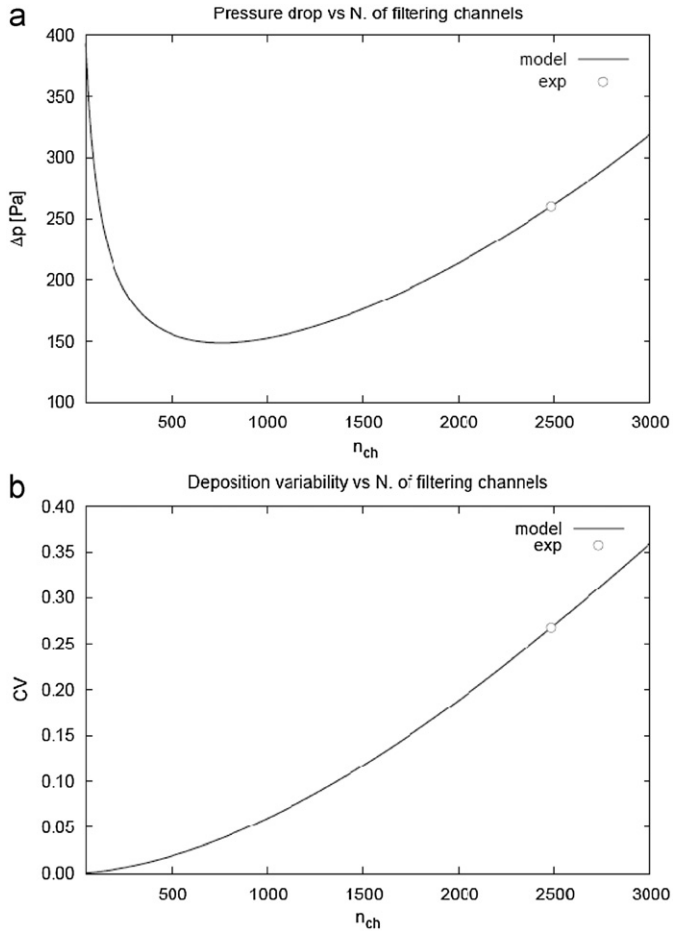

Fig. 7. Effect of number of filtering channels on filter performances: (a) pressure drop and (b) variability of deposition along filter.

the filter is fixed and the design choice can be to divide the filtering section into a few or a lot of channels having the same wall thickness. If a large number of channels is used, a large wall filtration area is obtained, but each channel has a small cross section. In these conditions, the pressure drop across the porous wall should decrease, but the friction along the channel is expected to increase. This behavior is predicted by the model, as shown in Fig. 7 where the variation of pressure drop as a function of the number of filtering channels shows a minimum. The deposited soot coefficient of variation, *CV*, is found to be monotonically increasing with the number of channels. In this case, the model shows that there is an optimum number of channels corresponding to the minimal pressure drop and low values of coefficient of variation for the deposited soot.

5. Conclusions

A fully analytical model has been developed to predict the velocity profile, the pressure drop and the soot spatial deposition profile along the channel of a wall-flow filter during the early stages of the deposition process. The model is based on Navier–Stokes and continuity equations; Darcy law is used to describe the pressure drop across the filter.

Due to the small aspect ratio of the channel, equations can be simplified according to the lubrication theory. Assuming that the filter permeability is constant along the filter, which is true for a clean filter and for uniform soot deposition, an analytical solution for the flow variables has been derived. Functional relationships between flow variables (pressure, section averaged streamwise velocity and through-wall velocity) and filter design parameters (number of channels, channel size, specific permeability of filter material) can be used for the filter design optimization. The deposition of nanosize soot particles, which is controlled by the through-wall velocity (Sbrizzai et al., 2005), can be predicted solving the transport equation for the soot.

Functional relationships have been derived to predict (i) the soot spatial deposition profile along the channel and (ii) a synthetic measure of dis-homogeneity of soot deposition, which can be used to assess "a priori" how critical can be the control of filter behavior over time.

The predictions of the model compare well with those obtained from more complex three-dimensional simulations, thereby demonstrating that the essential physics is captured correctly.

The parametric relationships between filter design variables and operating conditions have been explored to devised strategies for filter design optimization. Results indicate that pressure drop and dis-homogeneity of soot deposition can be minimized by a proper choice of filter channel geometry (number of filtering channels, size of channel) and filter material (specific permeability of the porous medium).

Notation

A, B	constants [−]
$A_{\text{filtering}}$	porous wall filtering section [m^2]
$A_{\text{flow}}=(2H)^2$	channel cross section [m^2]
A_{unit}	area of unit element of the filter [m^2]
b, c	rectangular channel half-width and half height [m]
c_1, c_2, c_4	integration constants [Pa]
c_3	integration constant [Pa/m]
$C(x)$	soot concentration [kg/m^3]
x	streamwise coordinate [m]
H	channel half-width [m]
K	filter permeability [m/Pa s]
k_s	specific filter permeability [m^2]
L	channel length [m]
$\dot{m}$	soot mass flow rate [kg/s]
$\dot{m}_0$	soot mass flow rate at channel inlet [kg/s]
$\dot{m}_{dep,ul}$	mass of soot depositing per unit length of channel [kg/m s]
n_{ch}	number of dirty/clean filtering channels [−]
p_E	static pressure at outlet of clean channel [Pa]
p_I	static pressure at inlet of dirty channel [Pa]
$p(x)$	static pressure in dirty channel [Pa]
$q(x)$	static pressure in clean channel [Pa]
Q	flow rate [m^3/s]
R	ratio between channel cross section and filter unit element area [−]
RES	filter resistance [Pa s/m]
s	thickness of the porous wall [m]
$u(x, y)$	axial velocity in dirty channel [m/s]
$U(x)$	section averaged velocity in dirty channel [m/s]
U_∞	undisturbed velocity upstream of filter [m/s]
$v(x, y)$	axial velocity in clean channel [m/s]
$V(x)$	section averaged velocity in clean channel [m/s]
$w(x)$	through-wall flow velocity [m/s]
w_{uni}	through-wall flow velocity, average value [m/s]
y, z	wall-normal (spanwise and vertical) coordinates [m]
$\Delta p=p_I-p_E$	pressure drop along filter (channel inlet–outlet) [Pa]
Δp_{filter}	pressure drop along filter (housing inlet–outlet) [Pa]

Greek letters

$\alpha = c/b$ rectangular section aspect ratio [−]
$\varepsilon = 2H/L$ channel aspect ratio [−]
$\lambda = (12K\mu/H^3)^{0.5}$ coefficient in pressure equation [1/m]
μ fluid viscosity [Pa s]

Abbreviations

CV coefficient of variation of variable [−]
E expected value of variable
ST.DEV. standard deviation of variable

Appendix A. Mean velocity profile versus pressure drop in square channel

According to Bahrami et al. (2006), the exact relationship between section averaged velocity and pressure drop for a rectangular channel (width 2c, height 2b) can be calculated as

$$U = \left(-\frac{dp}{dx}\right)\frac{1}{\mu}\left[\frac{1}{3} - \frac{64\alpha}{\pi^5}\tanh\frac{\pi}{2\alpha}\right] \tag{A.1}$$

where $\alpha = c/b$ is the rectangular section aspect ratio. The first term in the square parenthesis corresponds to the plane channel flow. The second term represents the correction for the rectangular channel. For a square section, the second term equals 0.1918, i.e. under the same pressure drop per unit length, the section averaged velocity through a square channel ($2H$ wide) is about one half (0.4246) of the section averaged velocity through a plane channel ($2H$ plane distance).

The effect of the correction factor can be considered included into the estimated value of filter specific permeability.

Appendix B. Solution of pressure equation

Eq. (9) can be rewritten as

$$\frac{d^2(p+q)}{dx^2} = 0 \tag{B.1}$$

from which we obtain that the sum of the pressures is a linear function of the streamwise coordinate x

$$p(x) + q(x) = c_3 x + c_4 \tag{B.2}$$

Eq. (10) can be rewritten as

$$\frac{d^2(p-q)}{dx^2} - \frac{12K\mu}{H^3}(p(x) - q(x)) = 0 \tag{B.3}$$

and if we define $\lambda^2 = 12K\mu/H^3$ (1/m^2), the solution is given by

$$p(x) - q(x) = c_1\exp(\lambda x) + c_2\exp(-\lambda x) \tag{B.4}$$

Summing/subtracting Eqs. (A.2) and (A.4), we obtain the pressure variation along the dirty and clean channel (Eqs. (11) and (12)).

Appendix C. Calculation of integration constants

The boundary conditions described by Eqs. (13)–(16) correspond to the following linear system in the integration constants

$$c_1 + c_2 + c_4 = 2p_I \tag{C.1}$$

$$c_1\exp(\lambda L) + c_2\exp(-\lambda L) - c_3 L - c_4 = -2p_E \tag{C.2}$$

$$c_1\lambda\exp(\lambda L) - c_2\lambda\exp(-\lambda L) + c_3 = 0 \tag{C.3}$$

$$c_1\lambda - c_2\lambda - c_3 = 0 \tag{C.4}$$

The system can be solved by linear combination and back sostitution. If we define

$$A = \exp(-\lambda L) + 1 \tag{C.5}$$

$$B = \exp(\lambda L) + 1 \tag{C.6}$$

the integration constants can be written as follows

$$c_2 = 2(p_I - p_E)\frac{B}{2(A+B) + \lambda L(B-A)} \tag{C.7}$$

$$c_1 = \frac{A}{B}c_2 \tag{C.8}$$

$$c_3 = \lambda\frac{A-B}{B}c_2 \tag{C.9}$$

$$c_4 = 2p_I - \frac{A+B}{B}c_2 \tag{C.10}$$

It is also possible to refer to the overall pressure drop, $\Delta p = p_I - p_E$, with $p_I = p_E + \Delta p$.

Appendix D. Filter specific permeability, filter permeability and filter resistance

From Darcy law, the local through-wall flow is a function of the local pressure gradient across the porous medium, ∇p

$$w = -\frac{k_s}{\mu}\nabla p \tag{D.1}$$

where k_s is the specific permeability of the porous material, (m^2). The pressure gradient across the porous wall can be calculated as $\nabla p = (q(x) - p(x))/s$, where s is the thickness of the porous wall, to obtain

$$w = \frac{k_s}{\mu s}(p(x) - q(x)) = K\cdot(p(x) - q(x)) \tag{D.2}$$

The specific permeability k_s is a function of the material only, whereas the filter permeability K is a function also of filter geometry.

Filter resistance represents the pressure drop across the filter per unit velocity at the channel inlet. From Eq. (18), substituting the values of the integration constants, we obtain

$$U(0) = -\frac{H^2}{6\mu}\left[2\lambda c_2\left(\frac{A}{B} - 1\right)\right] = -\frac{2H^2}{3\mu}\,\frac{\lambda(A-B)(p_I - p_E)}{2(A+B) + \lambda L(B-A)} \tag{D.3}$$

which can be rearranged to give

$$p_I - p_E = \Delta p = -U(0)\frac{3\mu(2(A+B) + \lambda L(B-A))}{2H^2\lambda(A-B)} \tag{D.4}$$

from which we can define RES as

$$RES = -\frac{3\mu(2(A+B) + \lambda L(B-A))}{2H^2\lambda(A-B)} \tag{D.5}$$

RES is function of both the geometrical characteristics of the filter (s, L and H) and of the porous material (k_s).

Appendix E. Filter geometry and channel characteristics

Channel characteristics can be univocally calculated once the main filter dimensions are fixed. We assume that the filter is made of identical filtering units each made of a couple of channels. With reference to the variables indicated in Table 1, we can write

$$A_{unit} = \frac{\pi D_f^2}{4n_{ch}} = 2(2H + s)^2 \tag{E.1}$$

$$A_{flow} = (2H)^2 \tag{E.2}$$

The contraction ratio can be calculated as

$$R = \frac{A_{flow}}{A_{unit}} \tag{E.3}$$

and the porous wall filtering section is given by

$$A_{filtering} = 8 n_{ch} HL \tag{E.4}$$

Reference "homogeneous" filtering conditions can be calculated as follows:

- through-wall filter velocity

$$w_{uni} = \frac{Q}{A_{filtering}} \tag{E.5}$$

- mass of soot deposited under uniform conditions

$$\dot{m}_{uni} = \frac{\dot{m}_0}{A_{filtering}} \tag{E.6}$$

References

Adler, J., 2005. Ceramic diesel particulate filters. Int. J. Appl. Ceram. Technol. 2, 429–439.

Ambrogio, M., Saracco, G., Specchia, V., 2001. Combining filtration and catalytic combustion in particulate traps for diesel exhaust treatment. Chem. Eng. Sci. 56, 1613–1621.

Ambrogio, M., Saracco, G., Specchia, V., van Gulijk, Makkee M., Moulijn, J.A., 2002. On the generation of aerosol for diesel particulate filtration studies. Sep. Purif. Technol. 27, 195–209.

Bahrami, M., Yovanovich, M.M., Culham, J.R., 2006. Pressure drop of fully developed laminar flow in microchannels of arbitrary cross section. J. Fluids Eng.—ASME Trans. 128, 1036–1044.

Bensaid, S., Marchisio, D.L., Fino, D., Saracco, G., Specchia, V., 2009a. Modelling of diesel particulate filtration in wall-flow traps. Chem. Eng. J. 154, 211–218.

Bensaid, S., Marchisio, D.L., Fino, D., 2010. Numerical simulation of soot filtration and combustion within diesel particulate filters. Chem. Eng. Sci. 65, 357–363.

Bensaid, S., Marchisio, D.L., Russo, N., Fino, D., 2009b. Experimental investigation of soot deposition in diesel particulate filters. Catal. Today 147, 295–300.

Chen, K., Martirosyan, K.S., Luss, D., 2009a. Soot combustion dynamics in a planar diesel particulate filter. Ind. Eng. Chem. Res. 48, 3323–3330.

Chen, K., Martirosyan, K.S., Luss, D., 2009b. Wrong-way behavior of soot combustion in a planar diesel particulate filter. Ind. Eng. Chem. Res. 48, 8451–8456.

Dabhoiwala, R. H., Johnson, J., Naber, J., Bagley, S., 2008. "A methodology to estimate the mass of particulate matter retained in a catalyzed particulate filter as applied to active regeneration and onboard diagnostics to detect filter failures". SAE Paper no. 2008-01-0764. Presented at SAE 2008 World Congress, April 2008.

Fino, D., Saracco, G., Specchia, V., 2002. Filtration and catalytic abatement of diesel particulate from stationary sources. Chem. Eng. Sci. 57, 4955–4966.

Fino, D., Fino, P., Saracco, G., Specchia, V., 2003. Innovative means for the catalytic regeneration of particulate traps for diesel exhaust cleaning. Chem. Eng. Sci. 58, 951–958.

Konstandopoulos, A.G., Papaioannou, E., 2008. Update on the science and technology of diesel particulate filters. Kona-Powder Part. 26, 36–65.

Liu, Y., Gong, J., Fu, J., Cai, H., Long, G., 2009. Nanoparticle motion trajectories and deposition in an inlet channel of wall-flow diesel particulate filter. J. Aerosol Sci. 40, 307–323.

Masoudi, M., 2005. Pressure drop of segmented diesel particulate filters. SAE 2005-01-0971.

Phares, D.J., Sharma, G., 2006. A DNS study of aerosol deposition in a turbulent square duct flow. Aerosol. Sci. Technol. 40, 1016–1024.

Pidria, M.F., Parussa, F., Merlone Borla, E., 2007. Mapping of diesel soot regeneration behaviour in catalysed silicon carbide filters. Appl. Catal. B: Environ. 70, 241–246.

Shende, A. S., Johnson, J. H., Yang, S. L., Bagley, S. T., Thalagavara, A. M., 2005. The filtration and particulate matter oxidation characteristics of a catalyzed wall-flow diesel particulate filter: experimental and 1-D 2-layer model results. SAE Paper no. 2005-01-0949. Presented at SAE 2005 World Congress, April 2005.

Sharma, G., Phares, D.J., 2006. Turbulent transport of particles in a straight square duct. Int. J. Multiphase Flow 32, 823–837.

Saracco, G., Badini, C., Specchia, V., 1999. Catalytic traps for diesel particulate control. Chem. Eng. Sci. 54, 3035–3041.

Saracco, G., Russo, N., Ambrogio, M., Badini, C., Specchia, V., 2000. Diesel particulate abatement via catalytic traps. Catal. Today 60, 33–41.

Sbrizzai, F., Verzicco, R., Pidria, M.F., Soldati, A., 2004. Mechanisms for selective radial dispersion of microparticles in the transitional region of a confined turbulent round jet. Int. J. Multiphase Flow 30, 1389–1417.

Sbrizzai, F., Faraldi, P., Soldati, A., 2005. Appraisal of three-dimensional numerical simulation for sub-micron particle deposition in a micro-porous ceramic filter. Chem. Eng. Sci. 60, 6551–6563.

Sbrizzai, F., Verzicco, R., Soldati, A., 2009. Turbulent flow and dispersion of inertial particles in a confined jet issued by a long cylindrical pipe. Flow Turbulence Combust. 82, 1–23.

Schejbal, M., Marek, M., Kubicek, M., Koci, P., 2009. Modelling of diesel filters for particulates removal. Chem. Eng. J. 154 (1–3), 219–230.

Yang, J., Stewart, M., Maupin, G., Herling, D., Zelenyuk, A., 2009. Single wall diesel particulate filter (DPF) filtration efficiency studies using laboratory generated particles. Chem. Eng. Sci. 64, 1625–1634.